



Influence of ionic liquid (IL) treatment conditions in the regeneration of cellulose with different crystallinity

Md. Mohosin Rana¹, Hector De la Hoz Siegler^{1,2,a)} 

¹Department of Biomedical Engineering, Schulich School of Engineering, University of Calgary, Calgary, AB T2N 1N4, Canada

²Department of Chemical and Petroleum Engineering, Schulich School of Engineering, University of Calgary, Calgary, AB T2N 1N4, Canada

^{a)}Address all correspondence to this author. e-mail: h.siegler@ucalgary.ca

Received: 1 July 2022; accepted: 14 October 2022; published online: 28 November 2022

In this study, we treated microcrystalline cellulose (MCC) with the ionic liquid (IL) 1-butyl-3-methylimidazolium chloride (BMIMCl) to elucidate the effects that IL treatment conditions have on the properties of amorphized cellulose (AC). Analysis of X-ray diffractograms confirmed that after 20 min of IL treatment AC crystallinity was reduced from 77.7 to 57.1%. After 10 h of IL treatment, AC crystallinity decreased to 29.6%. Chemical and morphological changes in the regenerated AC were determined via FT-IR and SEM studies. The rapid transformation of crystalline cellulose domains into amorphous domains is linked to the small MCC particle size (20 μm) and the presence of a moisture-free condition during IL treatment. Thermal stability of the treated cellulose, as determined by TGA and DSC profiling, decreased as the crystallinity index decreased. The high tunability of cellulose crystallinity by IL treatment provides a facile way for designing more efficient hybrid bioactive materials for biomedical applications.

Introduction

Cellulose is a naturally abundant polymer that can be isolated from different sources, such as plants, green algae, agro-industrial waste, and bacteria. There is an increasing interest in cellulose as a bioactive material for various biomedical applications due to its biocompatibility, favorable mechanical strength, and ease of integration with other materials. For example, Liu et al. synthesized a cellulose-based copolymer by grafting poly(N-isopropyl acrylamide) (PNIPAm) to methylcellulose (MC; a cellulose derivative) [1]. The resulting PNIPAm-g-MC hydrogels exhibited stronger thermal responsiveness than PNIPAm hydrogels. The mechanical properties of the hydrogels were also enhanced by tuning the ratio of PNIPAm and MC, thus, enhancing their potential as blood vessel barriers. In another study, cellulose nanocrystals (CNC) were incorporated with PNIPAm via both covalent and non-covalent interactions to synthesize PNIPAm-CNC hybrid hydrogels [2]. This hybrid hydrogels showed clear thermoresponsive behavior and stronger mechanical properties than PNIPAm hydrogels. Moreover, the incorporated CNC provided higher structural integrity upon injection for wound dressing applications.

The physical and chemical behavior of cellulose is strongly influenced by the arrangement of crystalline and amorphous domains. In cellulose, each anhydroglucose unit has three different hydroxyl groups. The hydroxyl groups at O(2) H, O(3) H, and O(6) H are the main reactive groups amenable to chemical modification (Fig. 1) [3]. During the chemical reaction, the accessibility of these hydroxyl groups on the cellulose fibril surface is a pivotal factor. Crystalline cellulose (CC) and microcrystalline cellulose (MCC) have highly ordered crystalline regions formed by strong hydrogen bonds [4]. Thereby, the compact structure of CC limits the accessibility of reactive hydroxyl groups [5]. For example, the O(3) H is unreactive to chemical reagents when the cellulose surface is highly ordered (Fig. 1) [3]. In contrast, the hydroxyl groups are accessible and reactive in the amorphized cellulose (AC), where the cellulose surface is mostly less ordered (Fig. 1). Despite the unreactive feature of the cellulose crystalline region, it provides enhanced mechanical strength to the polymer structure [6]. The mass ratio of crystallinity in cellulose is expressed as the crystallinity index (CrI). The CrI has an influence on the stiffness and rigidity of cellulose [7]. Therefore, cellulose with an appropriate CrI will enable the development of mechanically strong

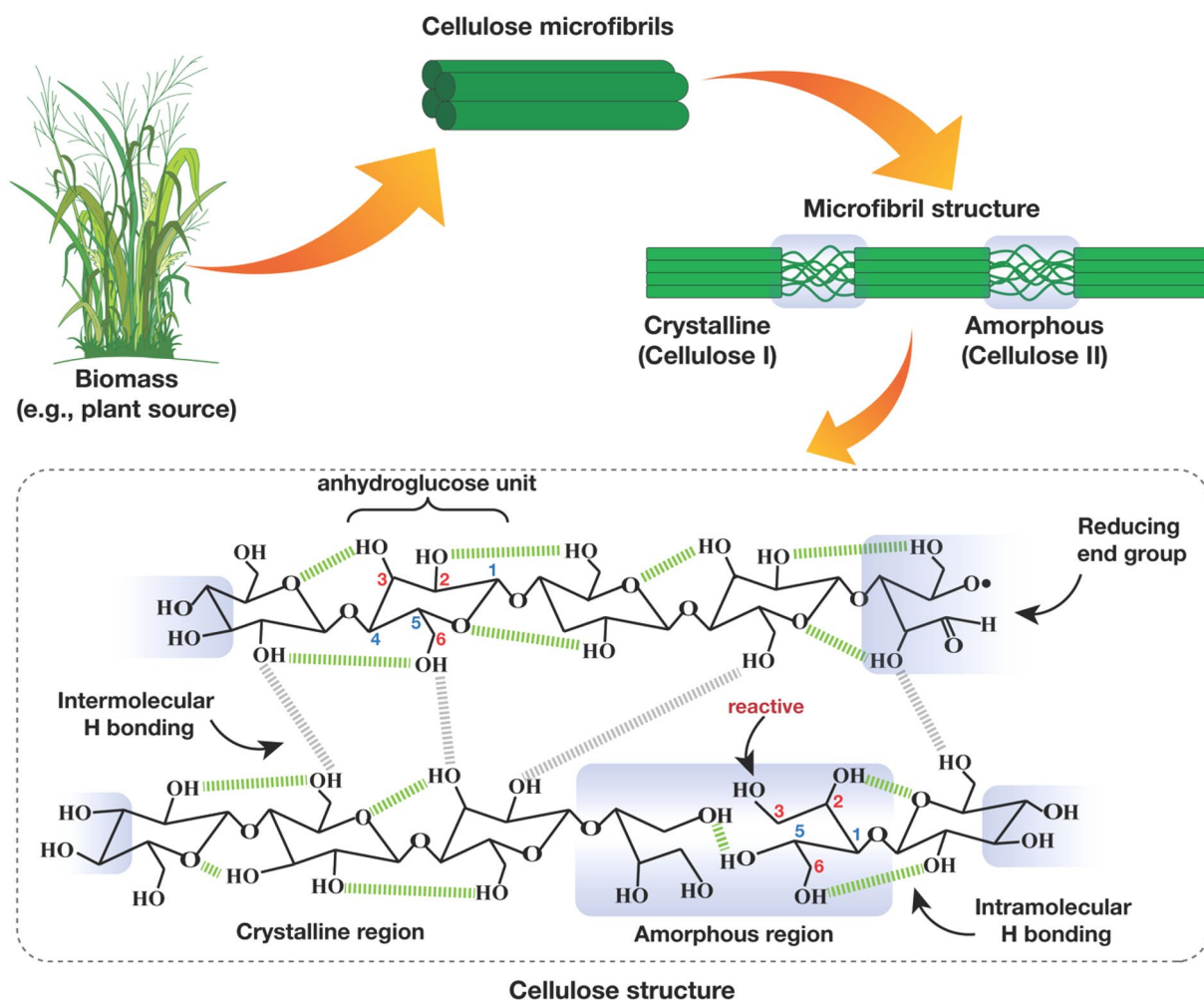


Figure 1: Molecular structure of cellulose obtained from biomass (e.g., plant source). Cellulose microstructure contains less reactive compact crystalline region and highly reactive amorphous region.

hybrid bioactive materials for different applications. For example, the presence of reducing functional groups in AC made it suitable to serve as a carrier of therapeutic substances for wound and burn treatments [8]. AC can also be used to develop mechanically strong hybrid scaffolds for tissue engineering applications [9]. Furthermore, the increased hydrophilicity, reactivity, accessibility, and enzymatic digestibility of AC have spurred the exploration of potential applications in agriculture [10].

Native cellulose from different sources have a wide range of crystallinity (e.g., CrI of sugarcane bagasse, soy hulls, wheat straw, and bacterial microcrystalline cellulose are 50, 69.6, 77.8, and 82.4%, respectively) [11, 12]. Chemical and mechanical treatments can be used to tune the crystallinity of cellulose as per the application requirement. For instance, acid hydrolysis is commonly used to produce CC [13]. In contrast, mechanical methods including high-pressure homogenization [14], grinding [15], cryocrushing [16], and ultrasonic techniques [17] are performed using high shear forces to produce AC [14, 18].

Despite the potential of these approaches, low productivity and high energy consumption limit their application.

Different solvent treatments have been developed to modify cellulose and its derivatives at milder conditions. Although solvent systems like *N,N*-dimethylacetamide (DMAc)/lithium chloride (LiCl), *N*-methyl-morpholine-*N*-oxide (NMMO)/water, sodium hydroxide (NaOH)/urea, and dimethyl sulfoxide (DMSO)/paraformaldehyde have been successfully used to treat cellulose, there is a very limited adoption of these solvents due to toxicity, high cost, limited dissolving ability, uncontrolled side reactions, and limited stability during cellulose modification [19, 20]. Ionic liquids (ILs) are organic salts with melting points below 100 °C and are regarded as green solvents [21, 22]. ILs have several advantages including lower volatility, non-flammability, good dissolving and extracting ability, good thermal stability, easy recyclability, and lower viscosity [23]. Hence, ILs have emerged as promising green solvents to produce AC from different biomass feedstocks [21, 24].

ILs can disrupt the native cellulose crystalline structure and break structurally important chemical linkages (e.g., β -1,4-glycosidic linkage). Furthermore, the cellulose dissolution conditions in ILs are relatively mild. For instance, cellulose dissolution in ILs (having low melting points) occurs at relatively low temperatures (25–100 °C), due to the lower viscosities of these ILs [25]. Thus, IL treatment can potentially replace mechanical treatment methods resulting in a more energy efficient method for AC production. A wide range of ILs, such as tetrabutylphosphonium acetate ($[P_{4444}] [Ac]$), 1-butyl-3-methylimidazolium chloride (BMIMCl), 1-allyl-3-methylimidazolium chloride (AMIMCl), and 1-ethyl-3-methylimidazolium chloride (EMIMCl) have been successfully used to dissolve cellulose [26]. BMIMCl is quite attractive, as it exhibits the highest hydrogen bonding basicity among commonly used ILs. The enhanced hydrogen bond accepting ability of Cl^- of BMIMCl results in strong interactions with the hydroxyl protons in cellulose, hence, leading to easier cellulose dissolution [27]. Several studies reported the transformation of cellulose I into cellulose II using BMIMCl, but the rate of cellulose amorphization (or decrystallization) in these studies is slow, and changes in CrI are low [28]. For instance, when highly crystalline cellulose (Avicel) was dissolved with BMIMCl and later regenerated, the crystallinity index (CrI) decreased from 76% in the original fibers to 65.4% in the case of fibers that have been dissolved in BMIMCl for 10 h [29].

Therefore, in this study, we investigate the effect that BMIMCl treatment time has on crystallinity, thermal properties, and the chemical structure of cellulose. Moreover, we explore modifications to the treatment conditions to increase the rate of the amorphization process and maximize the reduction in CrI.

Results and discussion

Cellulose crystallinity analysis

Changes in the cellulose structure result in distinctive XRD patterns. XRD spectra of all AC_x (where $x = 20$ min, 1, 3, 6, and 10 h of IL treatment, respectively) and MCC samples are depicted in Fig. 2. The untreated MCC has two peaks at around $2\theta = 15^\circ$ and 22.7° , corresponding to the (1-10) and (002) lattice planes. These are representative crystalline peaks of cellulose I [30]. For AC_{1h} , the peak shifts from $2\theta = 22.7^\circ$ to 22.4° , which reflects the (020) plane of cellulose II [31]. Such conversion usually depends on treatment conditions and type of biomass or IL used. The peak shift remained constant in samples treated for 3 h (AC_{3h}), 6 h (AC_{6h}), and 10 h (AC_{10h}). Moreover, along with the cellulose allomorph transformation, the decline in peak height with increasing treatment time indicates the conversion of crystalline structures to amorphous regions. Also, the appearance of peaks for 110 lattice planes ($2\theta = 15.6^\circ$) reflects the transformation of cellulose I to cellulose II [31].

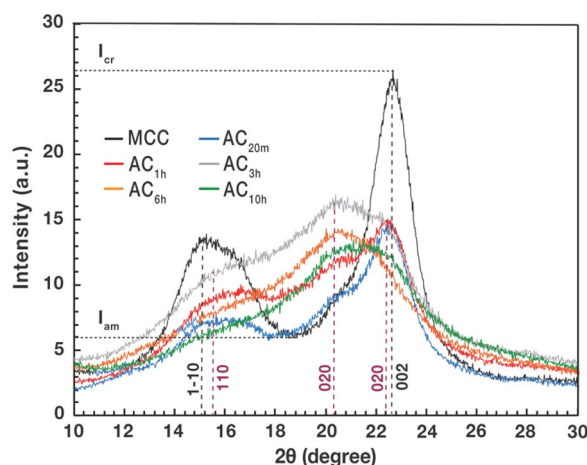


Figure 2: XRD diffractograms of untreated MCC and ACs obtained from different IL treatment duration. From the diffractograms, the fundamental peak (representative of the 002 lattice plane) consistently shifted with increasing IL treatment. Appearance of 020 (shifted peaks) and 110 lattice planes indicated the transformation of cellulose I to cellulose II.

TABLE 1: Crystallinity index (CrI) of untreated MCC and IL treated AC samples.

Sample	Treatment time	I_{cr}	I_{am}	Crystallinity index (CrI) (%)
MCC	0	26.5	6.03	77.7
AC_{20m}	20 min	14	6	57.1
AC_{1h}	1 h	15.1	8.8	41.7
AC_{3h}	3 h	16.9	11.4	33.1
AC_{6h}	6 h	14.4	9.9	30.6
AC_{10h}	10 h	13.5	9.5	29.6

The crystallinity index (CrI) is an important factor affecting cellulose properties. The values of CrI of untreated MCC and treated AC_{20m} , AC_{1h} , AC_{3h} , AC_{6h} , and AC_{10h} are presented in Table 1.

Crystallinity of MCC reduced significantly after short treatment time in BMIMCl (20 min and 1 h). It is observed that around 20.6% crystallinity (from 77.7 to 57.1%, see Table 1) was reduced just after 20 min of BMIMCl treatment (AC_{20m}). In a previous report, the crystallinity of Avicel (commercial microcrystalline cellulose; particle size: $\sim 50 \mu m$) was reduced by only 8.4% after 1 h of treatment with BMIMCl at 120 °C [29]. Compared to this previous report, the crystallinity reduction was ten times faster in the present study. The faster amorphization rate in the present study are likely due to differences in the size of the untreated cellulose and the vacuum conditions during treatment. Here, cellulose with lower particle size ($\sim 20 \mu m$) become more accessible to the solvent, which increases the solubility and reactivity of cellulose [32]. Treatment under vacuum, on the other hand, promotes the creation of a moisture-free environment. The

presence of moisture can inhibit cellulose dissolution in IL, as water causes the solvation of the IL anions, resulting in less sustained interaction with cellulose [33, 34]. A moisture-free environment was created by implementing vacuum condition along with constant nitrogen purging. Hence, in this study, in addition to the high weight ratio of cellulose to BMIMCl, the lower particle size of MCC and the moisture-free conditions enabled the fast reduction in crystallinity just after 20 min of IL treatment. With longer treatment time, it is evident that more crystalline structure of MCC transformed into amorphous regions; with the CrI value of AC_{10h} after 10 h of IL treatment being just 29.6%, which is much lower than the original MCC (77.7%).

Cellulose morphology

Fibrillar characteristics of cellulose after IL treatment can be observed via SEM imaging. Figure 3 shows the results of SEM obtained for MCC and IL treated ACs. The fibrillation of cellulose can be clearly distinguished from the untreated cellulose. Cellulose with high crystallinity (MCC) has less fibrillation on the surface [Fig. 3(a)].

In contrast, cellulose samples showed greater presence of fibrils with the increase in IL treatment time. AC from higher IL

treatment time (AC_{10h}) presented higher organization of fibrils [Fig. 3(f)]. It is presumed that the cellulose sample was separated mostly into fibers after IL treatment for 10 h. As was proven by XRD analysis, increasing IL treatment time resulted in lower crystallinity index and more disorganized cellulose (higher content of amorphous or fibrillar domains). Morphology of cellulose samples from SEM imaging also supported similar results.

Chemical structure analysis

Fourier-transform infrared spectroscopy (FT-IR) is widely used in the analysis of the structure of cellulose [35]. The FT-IR spectra of all six samples (MCC, AC_{20m}, AC_{1h}, AC_{3h}, AC_{6h}, and AC_{10h}) are depicted in Fig. 4. The identical peaks in the 2921–2871 and at 3340 cm⁻¹ indicates that both untreated MCC and treated ACs preserves similar functional groups in each wavenumber.

The peak at 1641 cm⁻¹ corresponds to O–H bending of adsorbed water. Due to the strong cellulose-water interaction, water adsorbed during the cellulose regeneration step is very difficult to remove even after stringent drying conditions [36]. The peak at 1155 cm⁻¹ corresponds to the C–OH and C–O–C pyranose ring stretching vibration in cellulose.

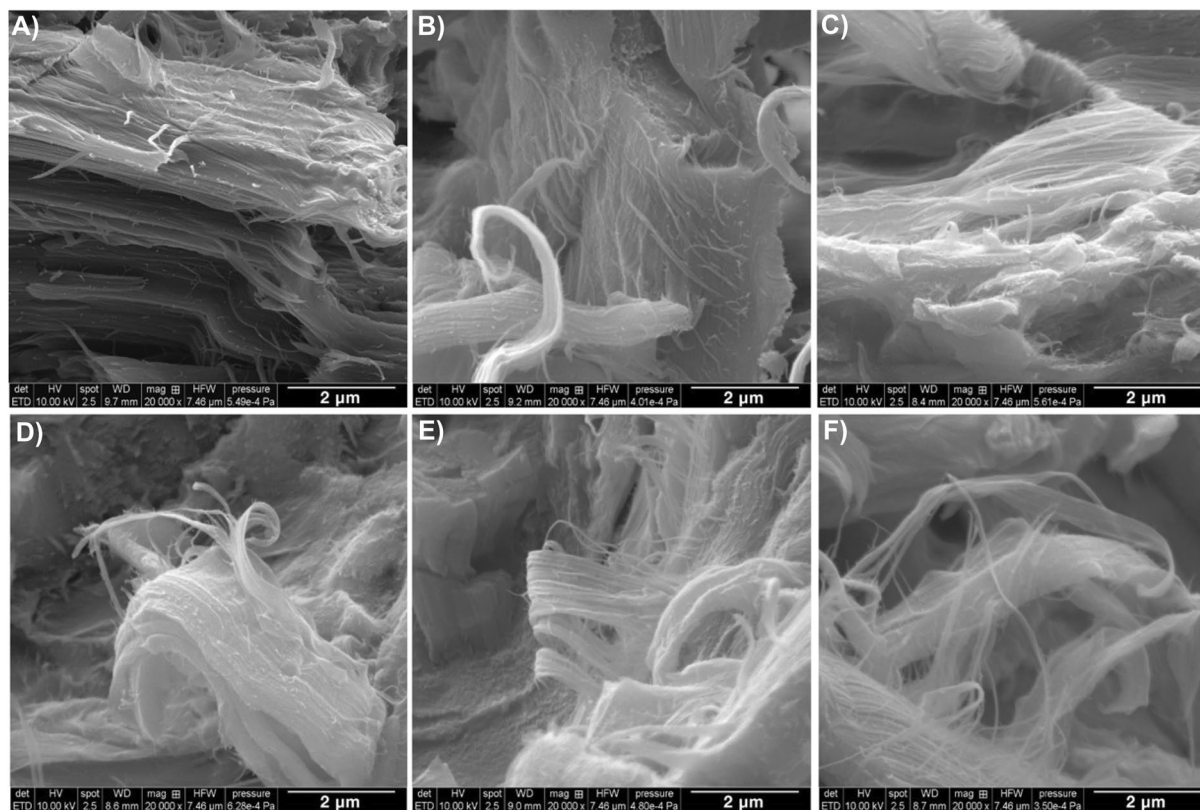


Figure 3: SEM images of cellulose samples. (a) untreated MCC, (b) AC_{20m}, (c) AC_{1h}, (d) AC_{3h}, (e) AC_{6h}, and (f) AC_{10h}. With the increase in IL treatment time, fibrillation of cellulose also increased (b–f).

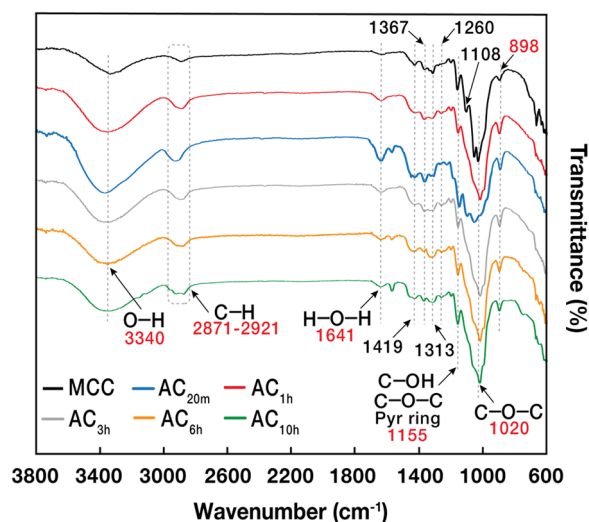


Figure 4: Comparative FT-IR spectra of MCC (untreated) and ACs from different IL treatment time. Peak strengths and absence/presence of peaks (representative of organic moieties of cellulose I and II) indicated the fibrillation and regeneration of ACs after various IL treatment time.

The C–C ring stretching band in cellulose can be seen in the peak at 1108 cm^{-1} . The peak at 1020 cm^{-1} is due to C–O–C stretching, while the typical absorption peak at 898 cm^{-1} represents C–O–C stretching vibration for β -glycosidic linkage of cellulose.

Structural changes can be seen in the $1500\text{--}850\text{ cm}^{-1}$ wavenumber region [37, 38]. The absorption peaks at 1108 and 1419 cm^{-1} are representative peaks for the C–C ring stretching and $-\text{CH}_2$ symmetric bending vibration in crystalline cellulose I. These peaks are sharp in the untreated MCC spectrum, which is highly crystalline, but in the spectra obtained from the BMIMCl treated samples, these peaks became weak, which indicates the dominance of amorphous regions in these samples. Moreover, the peaks at 1260 , 1313 , and 1367 cm^{-1} are representative peaks for $-\text{CH}$ bending vibration in cellulose II, $-\text{CH}_2$ wagging vibration in cellulose II, and $-\text{CH}$ bending vibration in both cellulose I and II, respectively. These peaks show a predominance of crystalline cellulose II in the BMIMCl treated AC samples, while these peaks are missing in the spectrum of untreated MCC sample. The absorption peak at 898 cm^{-1} , corresponding to the C–O–C stretching at β -glycosidic linkages of cellulose II, and predominant in the AC spectra while weak in the MCC spectrum.

The FT-IR of MCC and ACs are consistent with the previously reported FT-IR profiles of both commercial microcrystalline cellulose and regenerated cellulose [37, 39–41]. FT-IR confirms there were significant changes in the chemical structure of the originally microcrystalline cellulose. Moreover, the changes in the spectra support the hypothesis that there was a transition from cellulose I to cellulose II.

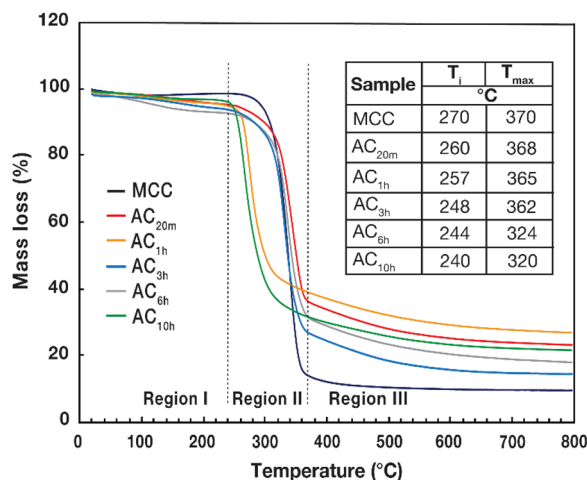


Figure 5: Thermogravimetric curves of MCC and IL treated AC samples. Three mass loss events were observed here. Major mass loss (Region II) of AC_{6h} and AC_{10h} started earlier compared to other due to the presence of higher amorphous domains.

Thermal stability study

Thermogravimetric analysis (TGA)

TGA curves of MCC and BMIMCl treated ACs are presented in Fig. 5. The TGA curves show that the thermal stability of the cellulose samples became less stable with increasing BMIMCl treatment time. All the samples exhibited nearly the same trend with three regions of thermal degradation. Region I, between 20 and 270 °C, is attributed to the vaporization of moisture with a slight mass loss [42]. It can be seen from the thermograms that the slight mass loss for MCC was extended to 270 °C, while other AC samples with different treatment time evaporated the moisture within 230–260 °C. This was associated with the presence of highest crystallinity in MCC compared to lower crystallinity of AC samples. This result is consistent with the XRD study as discussed in the previous section.

The major thermal degradation event (Region II) were started much earlier (from 230 °C) in AC_{3h}, AC_{6h}, AC_{10h} compared to MCC, AC_{20m}, and AC_{1h}. It is observed that the thermal stability decreased with increasing IL treatment time, which is reflected by the decrease in the initial temperatures (T_i) of the main mass loss event (Fig. 5). This is attributed to more disruption of crystalline regions of cellulose during BMIMCl treatment for longer time, resulted in decreased crystallinity. This in turn reduced the thermal resistance of the amorphized cellulose. The endpoint temperature (T_{max}) of this major mass loss event for MCC was 370 °C. The T_{max} gradually decreased with the IL treatment time in cellulose samples. The gradual decrease of the main thermal degradation event of IL treated ACs indicates that these cellulose samples displayed lower thermal stability than the untreated MCC.

Region III started at endpoint of region II (for each sample) up to 800 °C. This region mainly corresponded to the further

break down of thermal degradation intermediates, producing volatile materials like hydrogen, ethane, and ethylene [43].

Differential scanning calorimetric (DSC) analysis

The first and second order thermal transitions of cellulose samples, i.e., crystallization transition (T_c), glass transition (T_g), and thermal decomposition (T_d) were observed via DSC thermal analysis [44]. The DSC thermograms of all samples are shown in Fig. 6. For untreated MCC, the DSC curve exhibited an initial endothermic peak at approximately 120 °C which corresponds to the T_g for highly crystalline cellulose. The endothermic peak for glass transition temperature or T_g is prominent in polymers that contains higher ratio of amorphous region. In MCC, this early T_g value is due to the presence of a lower fraction of amorphous regions in its structure. The strong exothermic peak at around 340 °C represents the presence of a high degree of crystallinity in its structure [45], which is supported by the result obtained in XRD. Compared to untreated MCC sample, AC_{20m} and AC_{1h} also exhibited small exothermic peaks (representative of T_c for crystallinity) at around 175 and 256 °C, respectively. Despite this, all AC samples showed more prominent endothermic peaks which represents strong glass transition phenomenon during thermal analysis. All the five AC samples exhibited endothermic peaks within the temperature range between 269 and 340 °C. Interestingly, in the DSC curves of AC_{6h} and AC_{10h}, there are sharp endothermic peaks at approximately 269 and 278 °C, while no exothermic peaks are present in these two curves. This indicated the presence of highly amorphous regions in the cellulose structures due to the longer IL treatment time (6 and 10 h, respectively) [46]. This result further confirms the conclusions drawn from the XRD and TGA analyses as described earlier.

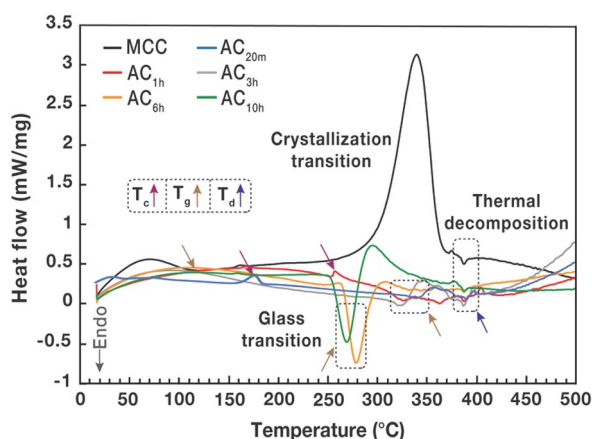


Figure 6: DSC thermograms of MCC and AC samples obtained from different IL treatment duration. From the thermograms, MCC, AC_{20m}, and AC_{1h} shows exothermic peaks indicative of crystallization transition due to the presence of significant number of crystalline domains. All the AC samples shows endothermic peaks representative of glass transition which confirms the presence of amorphous domains in their structure.

On the other hand, AC_{20m}, AC_{1h}, and AC_{3h} shows endothermic peaks (representative of T_g values) at higher temperatures, i.e., 340, 326, and 329 °C, respectively. The XRD study indicated that these samples (AC_{20m}, AC_{1h}, and AC_{3h}, respectively) shared a substantial portion of both crystalline and amorphous domains in their structure. Therefore, it is anticipated that due to the presence of significant ratios of crystallinity and amorphous regions, delayed endothermic peaks for T_g values were observed in their DSC curves. Moreover, it is important to note that DSC method is not a precise tool to determine the T_g of polymeric materials [46]. Hence, more precise thermal analysis tool (e.g., thermomechanical analysis or TMA, dynamic mechanical analysis or DMA) is needed in future to overcome the inconsistency of T_g values of a polymer obtained using different tools. Finally, an endothermic peak encountered at the later stage in all DSC thermograms (at around 384 °C) which represent thermal decomposition of cellulose samples. The decomposition temperatures were close to the onset thermal decomposition temperatures obtained from the region III in TGA thermograms. It is also clear from the thermal property analysis of untreated MCC, and IL treated ACs that the thermal stability was higher in highly crystalline cellulose (i.e., MCC). The BMIMCl treatment has significantly affected the thermal stability of cellulose. The thermal stability of the ACs reduced significantly with the decrease in cellulose crystallinity due to the BMIMCl treatment at various time duration. Therefore, MCC showed the highest thermal stability due to highest percentage of crystallinity, while AC_{10h} showed the lowest thermal stability because of lowest percentage of crystallinity.

Conclusion

During IL treatment, high vacuum environment was maintained along with nitrogen purging to keep high moisture-free environment for maximum cellulose dissolution. BMIMCl treatment of untreated cellulose substrate (MCC) at 100 °C for different treatment time (i.e., 20 min, 1, 3, 6, and 10 h) resulted in the gradual transformation of native cellulose crystalline I structure to cellulose II (highly amorphous). For all cases, the data indicate that IL treatment for all time variation resulted in the transformation from cellulose I to cellulose II lattice. Interestingly, just after 20 min of treatment, crystallinity of cellulose decreased dramatically from 77.7 to 57.1%. More than half of the crystalline regions of MCC transformed to amorphous regions after 3 h of IL treatment (i.e., 33.1%). Rapid decrease in the crystallinity up to 10 times (initial 20 min of treatment) faster than the previous report was observed in this study. The chemical characterization by FT-IR, morphology analysis by SEM, and thermal stability analysis also supported this drastic transformation from cellulose I to cellulose II after IL treatment. This study opens the

potential of ionic liquid treated cellulose with different crystallinity and amorphous ratio in mechanically strong hybrid material development for future biomedical applications.

Experimental methods

Materials

Microcrystalline cellulose (MCC, average diameter: 20 μm) and 1-butyl-3-methylimidazolium chloride (BMIMCl) were purchased from Sigma Aldrich. Nitrogen gas (purity: >99.999%) was purchased from Air Liquide Canada Inc. Deionized water (Resistivity: 18.2 $\text{M}\Omega/\text{cm} \pm 0.01 \text{ M}\Omega/\text{cm}$) was used for all the relevant experiments.

Dissolution of cellulose: IL treatment

For each dissolution experiment, cellulose (e.g., 1 g) was dried overnight in a vacuum dryer at 50 $^{\circ}\text{C}$ ($P = 20 \text{ kPa}$). Ionic liquid BMIMCl (e.g., 49 g) was added into a flask and stirred continuously under vacuum condition at 100 $^{\circ}\text{C}$ with nitrogen (N_2) gas purging to form clear solution. Dried cellulose with a weight ratio of 2% (cellulose to BMIMCl) was added into clear solution. This mixture was stirred at 100 $^{\circ}\text{C}$ under vacuum condition and N_2 purging for different time duration.

Operating at 100 $^{\circ}\text{C}$ provided a suitable balance between BMIMCl viscosity and energy consumption. The melting point of BMIMCl is about 70 $^{\circ}\text{C}$, but near this temperature, viscosity is too high, and a long time is required to achieve adequate dissolution of cellulose. As temperature increases, IL viscosity decreases. On the other hand, energy consumption will increase as temperature increases. Preliminary experiments at 85 $^{\circ}\text{C}$ indicated that viscosity was too high, and cellulose was not effectively dissolved, while at 100 $^{\circ}\text{C}$ there was no difficulty in achieving complete cellulose dissolution.

Treatment time varied from 20 min to 10 h. Preliminary experiments indicated that 20 min was the minimum time required for effective cellulose dissolution. As no significant changes were observed between samples treated for 6 or 10 h, longer treatment times were not further explored.

Regeneration of cellulose

After complete dissolution of cellulose in IL, the cellulose-BMIMCl mixture was slowly poured into water in 2:1 (water:BMIMCl) ratio with vigorous agitation at room temperature (25 $^{\circ}\text{C}$). The precipitate was collected by vacuum filtration and washed thoroughly with water via centrifugation to eliminate IL. The washed precipitate (regenerated cellulose) was then dried at 60 $^{\circ}\text{C}$ for 24 h and stored for subsequent experiments.

Crystallinity study: XRD analysis

The crystal structure of AC samples was studied by X-ray powder diffraction measurements using a model Bruker[®] D8 Advance diffractometer. The analysis was performed in the scattering angle range from 5 $^{\circ}$ to 60 $^{\circ}$ with 2 $^{\circ}/\text{min}$ scanning speed and a 2θ step interval of 0.05 $^{\circ}$ at room temperature. The crystallinity index (CrI) was calculated by,

$$\text{CrI} = \frac{I_{002} - I_{\text{am}}}{I_{002}} \times 100 \quad (1)$$

here, I_{002} is the maximum intensity of the (002) lattice diffraction, located around $2\theta = 22.5^{\circ}$ and represents crystalline region, I_{am} is the scattered intensity due to the amorphous part evaluated as the minimum intensity between the main and secondary peaks and located $2\theta = 18^{\circ}$ [47, 48].

Morphology analysis

SEM imaging was performed to check the effect of IL treatment on the cellulose crystallinity by comparing the surface morphology of untreated cellulose and regenerated cellulose (AC). The dried samples were then coated with platinum using a sputter coater to avoid subsequent charging before imaging by SEM.

Chemical structure analysis: FT-IR study

Spectroscopic study was conducted to observe the structural changes with the differences of crystallinity in dried untreated cellulose and ACs after IL treatment. For the FT-IR study, ATR unit with zinc selenide (ZnSe) crystals was used to record absorption spectra of 0.03 g sample using an FT-IR instrument (Bruker[®], model: Vertex 70). The scanning wavelength range for all samples were chosen between 600 and 3800 cm^{-1} .

Thermal stability study

The thermal stability of the untreated cellulose and AC samples were analyzed by thermogravimetric (TGA) differential scanning calorimetric (DSC) analysis using a thermal analyzer (Netzsch-Gerätebau GmbH, model: STA 409 PC/PG Luxx[®]). For TGA and DSC measurements, 0.01 g of samples were used under N_2 atmosphere with a gas flow of 60 mL/min by heating the material from 20 to 500 $^{\circ}\text{C}$ (for DSC) and 800 $^{\circ}\text{C}$ (for TGA) at a heating rate of 10 K/min.

Acknowledgments

This research was undertaken, in part, thanks to funding from the Canada First Research Excellence Fund (Grant No. CFREF-2015-00002). We want to thank the Department of

Chemistry and the Dynamic Imaging Laboratory of the University of Calgary for their technical support.

Author contributions

The manuscript was written through contributions of all authors. All authors have given approval to the final version of the manuscript.

Data availability

The data that support the findings of this study are available from the corresponding author upon reasonable request.

Declarations

Conflict of interest The authors declare there is no conflict of interest.

Open Access

This article is licensed under a Creative Commons Attribution 4.0 International License, which permits use, sharing, adaptation, distribution and reproduction in any medium or format, as long as you give appropriate credit to the original author(s) and the source, provide a link to the Creative Commons licence, and indicate if changes were made. The images or other third party material in this article are included in the article's Creative Commons licence, unless indicated otherwise in a credit line to the material. If material is not included in the article's Creative Commons licence and your intended use is not permitted by statutory regulation or exceeds the permitted use, you will need to obtain permission directly from the copyright holder. To view a copy of this licence, visit <http://creativecommons.org/licenses/by/4.0/>.

References

1. W. Liu, B. Zhang, W.W. Lu, X. Li, D. Zhu, K. De Yao, Q. Wang, C. Zhao, C. Wang, A rapid temperature-responsive sol-gel reversible poly(N-isopropylacrylamide)-g-methylcellulose copolymer hydrogel. *Biomaterials* **25**(15), 3005 (2004)
2. K. Zubik, P. Singhsa, Y. Wang, H. Manuspiya, R. Narain, K. Zubik, P. Singhsa, Y. Wang, H. Manuspiya, R. Narain, Thermo-responsive poly(N-isopropylacrylamide)-cellulose nanocrystals hybrid hydrogels for wound dressing. *Polymers (Basel)* **9**(12), 119 (2017)
3. C. Verlhac, J. Dedier, H. Chanzy, Availability of surface hydroxyl groups in valonia and bacterial cellulose. *J. Polym. Sci. A Polym. Chem.* **28**(5), 1171 (1990)
4. T. Shen, S. Gnanakaran, The stability of cellulose: a statistical perspective from a coarse-grained model of hydrogen-bond networks. *Biophys. J.* **96**(8), 3032 (2009)
5. V. Chunilall, T. Bush, P. T. Larsson, in *Cellulose - Fundamental Aspects*, edited by T. van de Ven and L. Godbout (IntechOpen, 2013), pp. 69–90.
6. D. Trache, A.F. Tarchoun, M. Derradji, T.S. Hamidon, N. Masruchin, N. Brosse, M.H. Hussin, Nanocellulose: from fundamentals to advanced applications. *Front. Chem.* **8**, 392 (2020)
7. O. S. Samuel and A. M. Adefusika, in *Cellulose*, edited by A. R. Pascual and M. E. E. Martin (IntechOpen, 2019), pp. 1–16.
8. M. Ioelovich, Preparation, characterization and application of amorphized cellulose—a review. *Polymers* **13**(24), 4313 (2021)
9. R.G.R. Brenes, M.A.B. Grieco, N. Bojorge, N. Pereira, Nanocellulose: production and processing for biomedical applications. *ChemNanoMat* **7**(12), 1259 (2021)
10. N.A.Z. Armir, A. Zulkifli, S. Gunaseelan, S.D. Palanivelu, K.M. Salleh, M.H.C. Othman, S. Zakaria, Regenerated cellulose products for agricultural and their potential: a review. *Polymers (Basel)* **13**(20), 3586 (2021)
11. S. Rongpipi, D. Ye, E.D. Gomez, E.W. Gomez, Progress and opportunities in the characterization of cellulose – an important regulator of cell wall growth and mechanics. *Front. Plant Sci.* **9**, 1894 (2019)
12. A. Khenblouche, D. Bechki, M. Gouamid, K. Charradi, L. Segni, M. Hadjadj, S. Boughali, Extraction and characterization of cellulose microfibrils from *Retama raetam* stems. *Polímeros* **29**(1), 1 (2019)
13. J. Gong, J. Li, J. Xu, Z. Xiang, L. Mo, Research on cellulose nanocrystals produced from cellulose sources with various polymorphs. *RSC Adv.* **7**(53), 33486 (2017)
14. M. Pääkko, M. Ankerfors, H. Kosonen, A. Nykänen, S. Ahola, M. Österberg, J. Ruokolainen, J. Laine, P.T. Larsson, O. Ikkala, T. Lindström, Enzymatic hydrolysis combined with mechanical shearing and high-pressure homogenization for nanoscale cellulose fibrils and strong gels. *Biomacromol* **8**(6), 1934 (2007)
15. H. Wang, S. Li, T. Wu, X. Wang, X. Cheng, D. Li, A comparative study on the characterization of nanofibers with cellulose I, I/II, and II polymorphs from wood. *Polymers* **11**(1), 153 (2019)
16. A. Chakraborty, M. Sain, M. Kortschot, Cellulose microfibrils: A novel method of preparation using high shear refining and cryocrushing. *Holzforschung* **59**(1), 102 (2005)
17. I. Filipova, V. Fridrihsone, U. Cabulis, A. Berzins, Synthesis of nanofibrillated cellulose by combined ammonium persulphate treatment with ultrasound and mechanical processing. *Nanomaterials* **8**(9), 640 (2018)
18. E.M. Podgorbunskikh, A.L. Bychkov, N.V. Bulina, O.I. Lomovskii, Disordering of the crystal structure of cellulose under mechanical activation. *J. Struct. Chem.* **59**(1), 201 (2018)
19. X. Liu, P.R. Chang, P. Zheng, D.P. Anderson, X. Ma, Porous cellulose facilitated by ionic liquid [BMIM]Cl: fabrication, characterization, and modification. *Cellulose* **22**(1), 709 (2015)

20. Y. Cao, J. Wu, J. Zhang, H. Li, Y. Zhang, J. He, Room temperature ionic liquids (RTILs): a new and versatile platform for cellulose processing and derivatization. *Chem. Eng. J.* **147**(1), 13 (2009)
21. J.K. Singh, R.K. Sharma, P. Ghosh, A. Kumar, M.L. Khan, Imidazolium based ionic liquids: a promising green solvent for water hyacinth biomass deconstruction. *Front. Chem.* **6**(Nov), 548 (2018)
22. Q.-L. Zhang, F. Shi, P. Wang, D.-Q. Lin, and S.-J. Yao, Preparation of cellulose adsorbents with ionic liquid and pore expansion for chromatographic applications. *J Appl. Polym. Sci.* **131**(7) (2014).
23. T. Aid, L. Paist, M. Lopp, M. Kaljurand, M. Vaher, An optimized capillary electrophoresis method for the simultaneous analysis of biomass degradation products in ionic liquid containing samples. *J. Chromatogr. A.* **1447**, 141 (2016)
24. D. Glas, R. Paesen, D. Depuydt, K. Binnemans, M. Ameloot, D.E. De Vos, R. Ameloot, Cellulose amorphization by swelling in ionic liquid/water mixtures: a combined macroscopic and second-harmonic microscopy study. *Chemsuschem* **8**(1), 82 (2015)
25. P. Mäki-Arvela, I. Anugwom, P. Virtanen, R. Sjöholm, J.P. Mikola, Dissolution of lignocellulosic materials and its constituents using ionic liquids—a review. *Ind. Crops Prod.* **32**(3), 175 (2010)
26. J. Zhang, J. Wu, J. Yu, X. Zhang, J. He, J. Zhang, Application of ionic liquids for dissolving cellulose and fabricating cellulose-based materials: state of the art and future trends. *Mater. Chem. Front.* **1**(7), 1273 (2017)
27. E. Amini, C. Valls, M.B. Roncero, Ionic liquid-assisted bioconversion of lignocellulosic biomass for the development of value-added products. *J. Clean. Prod.* **326**, 129275 (2021)
28. G. Laus, G. Bentivoglio, H. Schottenberger, V. Kahlenberg, H. Kopacka, T. Röder, H. Sixta, Ionic liquids: current developments, potential and drawbacks for industrial applications. *Lenzinger Berichte* **84**, 71 (2005)
29. Z. Ling, S. Chen, X. Zhang, K. Takabe, F. Xu, Unraveling variations of crystalline cellulose induced by ionic liquid and their effects on enzymatic hydrolysis. *Sci. Rep.* **7**(1), 1 (2017)
30. A.D. French, Idealized powder diffraction patterns for cellulose polymorphs. *Cellulose* **21**(2), 885 (2014)
31. K. Kobayashi, S. Kimura, E. Togawa, M. Wada, Crystal transition from cellulose II hydrate to cellulose II. *Carbohydr. Polym.* **86**(2), 975 (2011)
32. C. He, H. Li, J. Hong, H. Xiong, H. Ni, M. Zheng, Characterization and functionality of cellulose from pomelo fruitlets by different extraction methods. *Polymers* **14**(3), 518 (2022)
33. R.P. Swatloski, S.K. Spear, J.D. Holbrey, R.D. Rogers, Dissolution of cellose with ionic liquids. *J. Am. Chem. Soc.* **124**(18), 4974 (2002)
34. B. Crawford, A.E. Ismail, Insight into cellulose dissolution with the tetrabutylphosphonium chloride-water mixture using molecular dynamics simulations. *Polymers (Basel)* **12**(3), 627 (2020)
35. Y. Liu, Recent progress in fourier transform infrared (FTIR) spectroscopy study of compositional, structural and physical attributes of developmental cotton fibers. *Materials* **6**(1), 299 (2013)
36. J.I. Morán, V.A. Alvarez, V.P. Cyras, A. Vázquez, Extraction of cellulose and preparation of nanocellulose from sisal fibers. *Cellulose* **15**(1), 149 (2008)
37. Y.P. Yang, Y. Zhang, Y.X. Lang, M.H. Yu, Structural ATR-IR analysis of cellulose fibers prepared from a NaOH complex aqueous solution. *IOP Conf. Ser.* **213**, 012039 (2017)
38. M.L. Nelson, R.T. O'Connor, Relation of certain infrared bands to cellulose crystallinity and crystal lattice type. Part II. A new infrared ratio for estimation of crystallinity in celluloses I and II. *J. Appl. Polym. Sci.* **8**(3), 1325 (1964)
39. M.L. Nelson, R.T. O'Connor, Relation of certain infrared bands to cellulose crystallinity and crystal latticed type. Part I. Spectra of lattice types I, II, III and of amorphous cellulose. *J. Appl. Polym. Sci.* **8**(3), 1311 (1964)
40. F. Carrillo, X. Colom, J.J. Suñol, J. Saurina, Structural FTIR analysis and thermal characterisation of lyocell and viscose-type fibres. *Eur. Polym. J.* **40**(9), 2229 (2004)
41. H. Zhang, Y. Xu, Y. Li, Z. Lu, S. Cao, M. Fan, L. Huang, L. Chen, Facile cellulose dissolution and characterization in the newly synthesized 1,3-diallyl-2-ethylimidazolium acetate ionic liquid. *Polymers (Basel)* **9**(10), 526 (2017)
42. Y. Jiang, J. Zhou, Q. Zhang, G. Zhao, L. Heng, D. Chen, D. Liu, Preparation of cellulose nanocrystals from *Humulus japonicus* stem and the influence of high temperature pretreatment. *Carbohydr. Polym.* **164**, 284 (2017)
43. H. Yang, R. Yan, H. Chen, D.H. Lee, C. Zheng, Characteristics of hemicellulose, cellulose and lignin pyrolysis. *Fuel* **86**(12–13), 1781 (2007)
44. N.S. Malik, M. Ahmad, M.U. Minhas, Cross-linked β -cyclodextrin and carboxymethyl cellulose hydrogels for controlled drug delivery of acyclovir. *PLoS ONE* **12**(2), e0172727 (2017)
45. S. El-Sayed, K.H. Mahmoud, A.A. Fatah, A. Hassen, DSC, TGA and dielectric properties of carboxymethyl cellulose/polyvinyl alcohol blends. *Physica B* **406**(21), 4068 (2011)
46. R.R.M. de Freitas, A.M. Senna, V.R. Botaro, Influence of degree of substitution on thermal dynamic mechanical and physicochemical properties of cellulose acetate. *Ind. Crops. Prod.* **109**, 452 (2017)
47. G. Cheng, P. Varanasi, C. Li, H. Liu, Y.B. Melnichenko, B.A. Simmons, M.S. Kent, S. Singh, Transition of cellulose crystalline structure and surface morphology of biomass as a function of ionic liquid pretreatment and its relation to enzymatic hydrolysis. *Biomacromol* **12**(4), 933 (2011)
48. M.C. Dias, M.C. Mendonça, R.A.P. Damásio, U.L. Zidanes, F.A. Mori, S.R. Ferreira, G.H.D. Tonoli, Influence of hemicellulose content of Eucalyptus and Pinus fibers on the grinding process for obtaining cellulose micro/nanofibrils. *Holzforchung* **73**(11), 1035 (2019)